between the cellular automaton and the PDEs. It is not necessary to use the simulation results for tuning parameters, since all aspects of the automaton rule are derived from the PDE model. This approach is applicable to all PDE models that can be expressed in the form of (1), with a small parameter $0 < \epsilon \ll 1$. Since simulations of this automaton are computationally inexpensive compared to numerically solving the PDE, three dimensional calculations become more feasible.

REFERENCES

[1] M. Courtemanche, W. Skaggs and A. T. Winfree, *Stable three-dimensional action potential circulation in the FitzHugh-Nagumo model*, Phys. D, 41 (1990), pp. 173–182.

[2] V. G. Fast and I. G. Efimov, *Stability of vortex rotation in excitable cellular medium*, Phys. D, (submitted).

[3] R. J. Field and R. M. Noyes, *Oscillations in chemical systems IV. Limit cycle behavior in a model of a real chemical reaction*, J. Chem. Phys., 60 (1974), pp. 1877–1884.

[4] R. FitzHugh, *Impulse and physiological states in models of nerve membrane*, Biophysics J., 1 (1961), pp. 445–466.

[5] M. Gerhardt, H. Schuster and J. J. Tyson, *A cellular automaton model of excitable media including curvature and dispersion*, Science, 247 (1990), pp. 1563–1566.

[6] ———, *A cellular automaton model of excitable media including curvature and dispersion III. Fitting the Belousov-Zhabotinskii reaction*, Phys. D, 46 (1990), pp. 416–425.

[7] ———, *A cellular automaton model of excitable media including curvature and dispersion II. Curvature, dispersion, rotating waves and meandering waves*, Phys. D, 46 (1990), pp. 392–415.

[8] J. M. Greenberg, B. D. Hassard and S. P. Hastings, *Pattern formation and periodic structures in systems modeled by reaction-diffusion equations*, Bull. Am. Math. Soc., 84 (1978), pp. 1296–1327.

[9] J. M. Greenberg and S. P. Hastings, *Spatial patterns for discrete models of diffusion in excitable media*, SIAM J. Appl. Math., 34 (1987), pp. 515–523.

[10] W. Jahnke, W. E. Skaggs and A. T. Winfree, *Chemical vortex dynamics in the Belousov-Zhabotinskii reaction and in the two-variable Oregonator model*, J. of Physical Chem., 93 (1989), pp. 740–749.

[11] W. Jahnke and A. T. Winfree, *A survey of spiral wave behavoirs in the Oregonator model*, Intern. J. of Chaos and Bifurcations, (submitted).

[12] M. Markus, *Dynamics of a cellular automaton with randomly distributed elements*, in Mathematical Population Dynamics: Proc. Second Intern. Conf., Marcel Dekker, New York, NY, (in press).

[13] M. Markus and B. Hess, *Isotropic cellular automaton for modelling excitable media*, Nature, 347 (Sept. 1990), pp. 56–58.

[14] G. K. Moe, W. C. Rheinboldt and J. A. Abildskov, *A computer model of atrial fibrillation*, Am. Heart J., 67 (1964), pp. 200–220.

[15] J. J. Tyson, *A quantitative account of oscillations, bistability, and traveling waves in the Belousov-Zhabotinskii reaction*, in Oscillations and Traveling Waves in Chemical Systems, R. J. Fields and M. Burger, eds., Wiley, New York, 1985, pp. 93–144.

[16] J. J. Tyson and J. P. Keener, *Singular perturbation theory of traveling waves in excitable media (A review)*, Phys. D, 32 (1988), pp. 327–361.

[17] N. Wiener and A. Rosenblueth, *The mathematical formulation of the problem of conduction of impulses in a network of connected excitable elements, specifically in cardiac muscle*, Arch. Inst. Cardiol. de Mexico, 16 (1946), pp. 205–265.

[18] A. T. Winfree, *Spiral waves of chemical activity*, Science, 175 (1972), pp. 634–636.

[19] A. M. Zhabotinskii and A. N. Zaikin, *Concentration wave propagation in two-dimensional liquid-phase self-oscillating system*, Nature, 225 (1970), pp. 535–537.

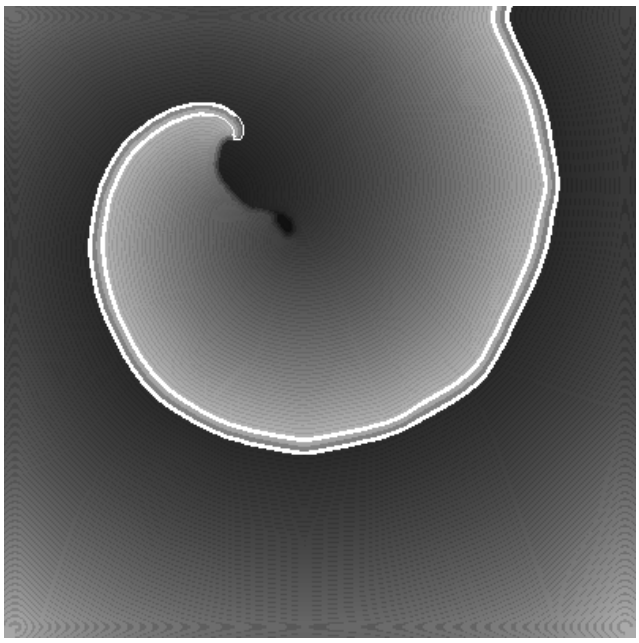

FIG. 3. *Spiral wave as calculated by the automaton.*

FIG. 4. *Motion of the tip of the spiral for t=3900 to t=4200.*

5. Parallel implementation. A parallel implementation on a ring connected multicomputer is straightforward: for p processors, the simulation domain is split into p strips of equal width. Each processor stores this strip plus two overlap areas each with a width equal to the radius of the mask. At the end of each cellular automaton step, which is carried out exactly as in the sequential implememtation, the information in the overlap areas is updated by messages between neighboring processors. This scheme is efficient as long as the width of each strip is larger than the size of the mask used.

6. Conclusion. A new way to construct a cellular automaton for simulating excitable media has been presented. The construction is based on singular perturbation analysis of the partial differential equation models for excitable media, and it shows the close relationship

Diffusion of the variable u and the excitation jump at the wavefront are simulated by using a big mask to count the number of excited cells in the neighborhood and applying a threshold function to the resulting (weighted) count Sum. This threshold function is selected such that the correct wave speed is obtained for all values of $\hat{v}$. Calculate from the PDE the planar wave speed $c = c_2(\hat{v})$ of an isolated front propagating into medium with recovery value $\hat{v}$. From the mask, a simulation gives the function $c_1(k)$, the planar wave speed as a function of the threshold (averaged over all directions). These two speeds should be equal (in their respective time and space scales) for all values of $\hat{v}$. Therefore

$$k(v) = c_1^{-1}\big(\alpha\, c_2\,(L^{-1}(v))\big).$$

Here L^{-1} is an affine transformation from the automaton variable v into the PDE variable $\hat{v}$ and α transforms the units of measurement for wave speeds.

So a rule for updating u in the automaton is:

$$\begin{aligned} &Sum := Mask * u^t \ ; \\ &\textbf{if } \ Sum > k(v) \textbf{ then } \ u^{t+1} = 1 \\ &\qquad\qquad\qquad \textbf{else } \ u^{t+1} = 0; \end{aligned}$$

where the superscript refers to the time step t and '*' denotes convolution.

The update function for v is obtained directly from the PDE for $\hat{v}$:

$$\frac{\partial \hat{v}}{\partial t} = \begin{cases} g(h_+(\hat{v}), \hat{v}) & \text{if } u = 1; \\ g(h_-(\hat{v}), \hat{v}) & \text{if } u = 0. \end{cases}$$

The rule for updating v in the automaton is:

$$\begin{aligned} &\textbf{if } \ v^t = v_{\text{maxaut}} \textbf{ then} \\ &\qquad\qquad u^{t+1} = 0 \\ &\textbf{else if } \ u^t = 0 \textbf{ then} \\ &\qquad\qquad v^{t+1} = \max\{0, v^t + \lfloor L'\, g_-(v)\, \Delta t \rfloor\} \\ &\textbf{else if } u^t = 1 \textbf{ then} \\ &\qquad\qquad v^{t+1} = \min\{v_{\text{maxaut}}, v^t + \lceil L'\, g_+(v)\, \Delta t \rceil\}, \end{aligned}$$

where $L' = dL/d\hat{v} = v_{\text{maxaut}}/(\hat{v}_{\max} - \hat{v}_{\min})$, $g_\pm = g\,(h_\pm(\hat{v}), \hat{v})$ with $\hat{v} = L^{-1}(v)$, and Δt is the length of one CA time step measured in PDE time units.

If v_{maxaut} is big, the error introduced by the discretization of $\hat{v}$ (the $\lfloor\ \rfloor$ and $\lceil\ \rceil$ operations) is small.

4. Spiral wave simulation. To complete the description of a CA model, the functions $f(\hat{u}, \hat{v})$ and $g(\hat{u}, \hat{v})$ in (1) must be specified. The Oregonator model is chosen:

$$f(\hat{u}, \hat{v}) = \hat{u}(1 - \hat{u}) - \hat{f}\hat{v}(\hat{u} - q)/(\hat{u} + q), \quad g(\hat{u}, \hat{v}) = \hat{u} - \hat{v},$$

with $\hat{f} = 3$ and $q = 0.002$. The values of the CA space constant and time step, Δx and Δt, measured in PDE units, are obtained by identifying (1) diffusion coefficients and (2) solitary plane wave speeds in the PDE and CA models. With all this machinery in place, a rotating spiral wave was calculated on a 400×400 grid of cells. A snapshot of a spiral is shown in Figure 3, where the region of excitation is outlined in white and the greylevels indicate the value of the recovery variable v. This CA simulation of the spiral wave shows many features that appear in simulations of the Oregonator PDEs by standard numerical methods [10], [11], even down to the "meandering" of the tip of the spiral (see Figure 4).

$$\text{Mask} = \begin{bmatrix}
0 & 0 & 0 & 0 & 1 & 1 & 1 & 1 & 1 & 1 & 1 & 0 & 0 & 0 & 0 \\
0 & 0 & 0 & 1 & 2 & 3 & 3 & 3 & 3 & 3 & 2 & 1 & 0 & 0 & 0 \\
0 & 0 & 1 & 2 & 4 & 5 & 6 & 6 & 6 & 5 & 4 & 2 & 1 & 0 & 0 \\
0 & 1 & 2 & 4 & 6 & 8 & 9 & 10 & 9 & 8 & 6 & 4 & 2 & 1 & 0 \\
1 & 2 & 4 & 6 & 9 & 11 & 13 & 13 & 13 & 11 & 9 & 6 & 4 & 2 & 1 \\
1 & 3 & 5 & 8 & 11 & 14 & 16 & 17 & 16 & 14 & 11 & 8 & 5 & 3 & 1 \\
1 & 3 & 6 & 9 & 13 & 16 & 19 & 20 & 19 & 16 & 13 & 9 & 6 & 3 & 1 \\
1 & 3 & 6 & 10 & 13 & 17 & 20 & 21 & 20 & 17 & 13 & 10 & 6 & 3 & 1 \\
1 & 3 & 6 & 9 & 13 & 16 & 19 & 20 & 19 & 16 & 13 & 9 & 6 & 3 & 1 \\
1 & 3 & 5 & 8 & 11 & 14 & 16 & 17 & 16 & 14 & 11 & 8 & 5 & 3 & 1 \\
1 & 2 & 4 & 6 & 9 & 11 & 13 & 13 & 13 & 11 & 9 & 6 & 4 & 2 & 1 \\
0 & 1 & 2 & 4 & 6 & 8 & 9 & 10 & 9 & 8 & 6 & 4 & 2 & 1 & 0 \\
0 & 0 & 1 & 2 & 4 & 5 & 6 & 6 & 6 & 5 & 4 & 2 & 1 & 0 & 0 \\
0 & 0 & 0 & 1 & 2 & 3 & 3 & 3 & 3 & 3 & 2 & 1 & 0 & 0 & 0 \\
0 & 0 & 0 & 0 & 1 & 1 & 1 & 1 & 1 & 1 & 1 & 0 & 0 & 0 & 0
\end{bmatrix}$$

FIG. 1. *Effective weights in the mask.*

D(k) : diffusion coefficient vs threshold.

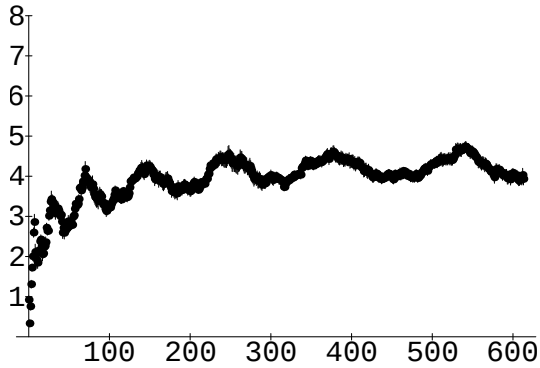

c(k) : speed vs threshold.

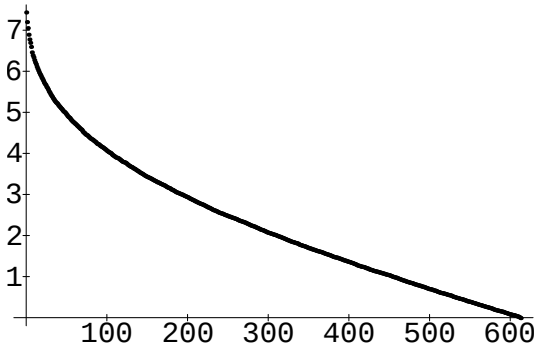

FIG. 2. *Diffusion coefficient and planar wave speed vs threshold for our Mask.*

3. within the wavefronts and wavebacks, $\hat{v}$ changes very little, since $\hat{v}$ is a slow variable. Solving the equation $f(\hat{u}, \hat{v}) = 0$ for $\hat{u}$ gives three solution branches,

$$\hat{u} = h_-(\hat{v}), \qquad \hat{u} = h_0(\hat{v}), \qquad \hat{u} = h_+(\hat{v}),$$

two of which ($h_-(\hat{v})$ and $h_+(\hat{v})$) are stable. These two branches determine the value of $\hat{u}$ in the regions between wavefronts and wavebacks.

The value of $\hat{v}$ is limited by $\hat{v}_{\min} \le \hat{v} \le \hat{v}_{\max}$, where $\hat{v}_{\min}$ is the value of $\hat{v}$ at the resting state, i.e., the stable solution of $g(\hat{u}, \hat{v}) = 0$ and $f(\hat{u}, \hat{v}) = 0$. Likewise, $\hat{v}_{\max}$ is the value of $\hat{v}$ at which $h_0(\hat{v}) = h_+(\hat{v})$. At this value of $\hat{v}$, $h_+(\hat{v})$ is not stable. At $\hat{v} = \hat{v}_{\max}$, a waveback occurs as a jump from $\hat{u} = h_+(\hat{v})$ to $\hat{u} = h_-(\hat{v})$.

In order to model a PDE of this sort, introduce two variables u, v in the cellular automaton:

$$u = \begin{cases} 0 & \textbf{if } \hat{u} = h_-(\hat{v}), \qquad \text{(recovering state)} \\ 1 & \textbf{if } \hat{u} = h_+(\hat{v}), \qquad \text{(excited state)} \end{cases}$$

and

$$v = L(\hat{v}) := \frac{\hat{v} - \hat{v}_{\min}}{\hat{v}_{\max} - \hat{v}_{\min}} v_{\text{maxaut}}.$$

In particular, $N = c + D\,K$, where N is the normal velocity, K is the curvature, D is the diffusion coefficient, and c is the planar wave speed.

- Dispersion relation: A wavefront can propagate not only into resting medium, but also into partially recovered medium. In this case the speed of the traveling wave should be slower than the speed of propagation into fully recovered (resting) medium.
- Spatial isotropy: The shape of spirals in these early models was always square, not round, due to the nearest-neighbor-only connections and the resulting anisotropic speed of propagation.

These three shortcomings have been addressed in "second generation" models by Gerhardt, Schuster and Tyson [5], [6], [7], Markus and Hess [12], [13], and Efimov and Fast [2].

To model curvature effects, Gerhardt, Schuster and Tyson introduced bigger neighborhoods. They used squares of size $(2r+1)^2$, where $r = 1, \cdots, 6$. In their automaton the number of excited cells within this square is counted and a threshold function is applied to the result. Furthermore, by making the threshold a linear function of the recovery state, they introduce dispersion. Their automaton still suffers somewhat from directional anisotropy.

Markus and Hess address the problem of directional anisotropy by introducing semi-random grids. They randomize the position of a grid point within its unit square, and then mark all neighbors within a circular boundary centered on the grid point. In this manner they achieve good isotropy at the cost of high computational complexity.

Efimov and Fast recognize that for determining whether a cell should become excited, the excitation of a nearby cell has a bigger effect than the excitation of a cell that is far away. They calculate a weighted sum of excitation of cells in the neighborhood, where cells close to the center have high weights and cells far away have low weights.

This paper introduces a "third generation" automaton that combines the strengths and avoids the weaknesses of these earlier versions. Furthermore, the cellular automaton (CA) rules are closely related to the underlying partial differential equations (1).

2. Description of new mask. Gerhardt, Schuster and Tyson used a square mask because the operation of counting the number of excited neighbors can be done in a time independent of the size of the mask. This property is very desirable, especially for big masks. The basic idea is to construct a square mask as the convolution of a vertical strip and a horizontal strip. The sum within a strip is calculated by a scanning operation.

Another mask (a diamond mask) can be constructed as the convolution of two diagonal strips. The new mask is calculated as the convolution of a square mask and a diamond mask. The results of its application to a data array can be calculated with 8 addition operations per cell, independent of the size of the mask. The examples here use a square mask of radius 3 and a diamond mask that is constructed from diagonal strips of length 5 (radius 2). The "combination" mask is shown in Figure 1.

A crucial test for this mask is the curvature relationship, $N = c + D\,K$, which is tested by simulations of waves with different curvatures. The mask exhibits a linear relationship with an effective diffusion coefficient of 4, almost independent of the threshold at which the speed of propagation is determined. Figure 2 summarizes the simulation results.

3. Construction of cellular automaton rules from the PDE model. In the PDE model (1), ϵ is a small (positive) parameter representing the time scales for changes in $\hat{u}$ (the fast variable) and $\hat{v}$ (the slow variable). The smallness of ϵ makes numerical solution of (1) difficult, but it can be exploited by singular perturbation theory [16] to show that

1. traveling wave solutions are possible for these systems;
2. away from the wavefronts and wavebacks $\hat{u}$ changes very little, so that $f(\hat{u}, \hat{v}) \approx 0$;

Proc. of the Fifth SIAM Conf. on Parallel Processing for Scientific Computation

J. Dongarra, ed.; SIAM, (1992) 376-381

THIRD GENERATION CELLULAR AUTOMATON FOR MODELING EXCITABLE MEDIA*

JÖRG R. WEIMAR† and JOHN J. TYSON‡ and LAYNE T. WATSON†

Abstract. This paper introduces a new cellular automaton model of excitable media with improved treatments of (1) diffusion and wave propagation, and (2) slow dynamics of the recovery variable. The automaton is both computationally efficient and faithful to the underlying partial differential equations.

1. Introduction. Excitable media support undamped traveling waves of excitation, such as waves of membrane depolarization in nerve axons and waves of star formation in galactic dust clouds. Traditionally, excitable media have been modeled either by partial differential equations or by cellular automata.

Some simple (two-variable) partial differential equation models of the form

$$\begin{aligned} \frac{\partial \hat{u}}{\partial t} &= \epsilon \nabla^2 \hat{u} + \frac{1}{\epsilon} f(\hat{u}, \hat{v}), \\ \frac{\partial \hat{v}}{\partial t} &= g(\hat{u}, \hat{v}), \end{aligned} \tag{1}$$

have become popular representations of excitable media, e.g., the Oregonator model [3], [10], [15] of the Belousov-Zhabotinskii reaction [18], [19], and the FitzHugh-Nagumo model [1], [4] of neuromuscular membranes. But the earliest model (1946) of excitable media was a cellular automaton introduced by Wiener and Rosenblueth [17]. The cellular automaton approach was pursued later by Moe at al. [14], Greenberg and Hastings [8], [9] and others. These "first generation models" featured nearest neighbor connections and only a few possible states per cell. Although they exhibited wave propagation, they failed in several crucial aspects:

- The curvature effect: A wavefront that is curved backward should travel slower than a planar wave, which in turn should be slower than a wavefront that is curved forward.

* This work was supported in part by National Science Foundation Grant DMS-8810456 and Department of Energy Grant DE-FG05-88ER25068..

†Department of Computer Science, Virginia Polytechnic Institute and State University, Blacksburg, Virginia 24061-0106.

‡Department of Biology, Virginia Polytechnic Institute and State University, Blacksburg, Virginia 24061-0406.